Applied Surface Science 678 (2024) 161128

Contents lists available at ScienceDirect

Applied Surface Science

journal homepage: www.elsevier.com/locate/apsusc

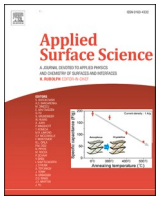

Full Length Article

Effect of Ni addition and bath temperature on electroless Cu microstructure in microvia preparation for HDI substrate

Zheng Zhang [a,*], Ming-Chun Hsieh [a], Masahiko Nishijima [a], Aiji Suetake [a], Hiroshi Yoshida [a], Rieko Okumuara [a], Chuantong Chen [a], Hiroki Seto [b], Kei Hashizume [b], Yuhei Kitahara [b], Haruki Nagamura [b], Katsuaki Suganuma [a]

[a] Flexible 3D System Integration Lab, SANKEN, Osaka University, 5670047, Japan
[b] Okuno Chemical Industries Co. Ltd, 5410045, Japan

ARTICLE INFO

Keywords:
Electroless Cu deposition
Microstructure
Nanovoids
Hydrogen bubbles
TEM observations

ABSTRACT

In this work, we investigated the microstructure evolution of electroless copper (Cu) deposition under different nickel (Ni) additions and reaction temperatures. It was found that the grain structure of electroless Cu is significantly influenced by the addition of Ni due to its inhibitory effect on Cu self-diffusion, while bath temperature had no impact on the electroless Cu grain growth. Additionally. nanovoids were observed in the electroless layer, primarily at the interface between the Cu trace and electroless layer, which is caused by the attachment of hydrogen bubbles during the electroless Cu reaction. These nanovoids do not affect the epitaxial grain growth in the microvia structure as observed through transmission electron microscopy (TEM). The nanovoids in the electroless Cu under different deposition conditions were also investigated through TEM images with the assistance of ImageJ. We found that the dimension of nanovoids initially increases with the reaction rate, as a result of the higher deposition rate introducing large hydrogen bubbles. However, as the reaction rate further increases, the size of the nanovoids stabilizes because larger hydrogen bubbles more easily escape the surface. This work may offer insights into potential approaches to enhance the quality of electroless Cu deposition for microvia preparation.

1. Introduction

Electroless copper (Cu) deposition is a widely utilized surface coating method to achieve a thin and uniform Cu layer on various solid surfaces [1–3]. In contrast to electrolytic copper deposition, which relies on an electrical reaction by passing an electric current through the bath and substrate, electroless deposition is dependent on reduction of Cu ions through an autocatalytic reaction. This unique characteristic allows for the formation of an even Cu layer on the different surfaces regardless of their geometry and conductivity. One of the most important applications of electroless Cu deposition is in the manufacturing of printed circuit boards (PCBs). The electroless Cu layer is plated on the drilled structures and laminated films of PCBs, severing as a conductive seed layer for the consequent Cu electroplating to form circuit traces and via structures.

Recently, the quality of the electroless Cu has gained more attention due to increasing demand for high-density interconnect (HDI) substrate – a type of high-end PCB substrate with higher input/output density [4–6]. The traces and vias in the HDI substrates that need to be electroless plated are becoming smaller and more delicate to meet the increased numbers of input/output and complex design of the HDI substrate. The electroless Cu layer of the HDI substrate is susceptible to high stress caused by coefficients of thermal expansion (CTE) mismatch among metallic circuits, hard cores, and dielectric film. In 2018, IPC released a white paper (IPC-WP-023) [7] highlighting a trend of failure occurring at the interface between the Cu trace and microvia, precisely where the electroless layer is located. It is also reported that delimitation occurs at the interface between the Cu trace and microvia even after a few times of solder reflows due to the poor quality of the electroless Cu deposition [8]. In the manufacturing of microvia, a thin electroless Cu layer (0.3 ~ 1 μm) is deposited on the surfaces of drilled holes for a consequent electrolytic Cu deposition. Thus, the microvia is a Cu trace/electroless Cu/electrolytic Cu sandwich structure, and the quality of the electroless Cu layer is critical to the interconnection quality between the Cu trace and microvia structure, particularly as the size of the microvia

* Corresponding author.
E-mail address: zhangzheng@sanken.osaka-u.ac.jp (Z. Zhang).

https://doi.org/10.1016/j.apsusc.2024.161128
Received 10 June 2024; Received in revised form 21 August 2024; Accepted 29 August 2024
Available online 30 August 2024

is becoming samller in the HDI substrates.

At present, co-evolution of hydrogen gas is regarded as one of the biggest challenges of electroless Cu since it can significantly impact the microstructures of Cu deposition layer due to hydrogen bubble inclusion. In the reaction of electroless Cu deposition, Cu^{2+} ions get reduced on the plated surface under the effects of catalyst and reducing agents, while an equivalent molar amount of hydrogen gas can be simultaneously generated during the reaction. The hydrogen gas gets trapped and forms hydrogen bubbles on the plated surface, leading to nano- and micro-voids in the electroless Cu deposition[9–11]. The mechanical properties of electroless Cu can be thus significantly degraded under the influence of these voids [12,13]. The influence of these voids is much more prominent in the microvia structure that provides interconnection among different buildup layers of HDI substrate.

To reduce the nanovoids in the electroless Cu deposition layer, extensive research has been conducted on the evolution of hydrogen in the electroless Cu reaction. One of the efficient and popular methods to diminish the H_2 evolution during Cu electroless deposition in the PCBs industry is by adding a small amount of nickel (Ni) addition[14]. The evolution of H_2 can be significantly suppressed by the synergistic effect of oxidation intermediate caused by the Ni addition that can partially convert H radicals into monovalent hydrogen in the form of H_2O, rather than the H_2 gases [15]. Seo et al. [16] reported that blister formation on an organic substrate can be significantly prevented by the Ni addition due to its suppression effect on H_2 evolution. In addition, Tobias et al. [17] propose that the incorporation of Ni^{2+} in the deposition can prevent the encapsulation of H_2 bubbles during Cu grain growth. They suggest that Ni can facilitate a horizontal growth direction of Cu grains, thereby reducing the encapsulation of H_2 under a vertical growth mode. However, the H radicals cannot be completely converted into the form of H_2O under the effect of Ni [18]. Nanosized voids that are less than 100 nm still extensively exist in the Cu electroless deposition according to transmission electron microscopy (TEM) observations, which is still a potential risk for microvia structure [19]. Recently, Park et al [20] directly deposited Cu on a Si_3N_4 TEM grid and quantified the nanovoids in the electroless layer at the initial stage. It is found that the reduction in both reaction temperature and reducing agent concentration can result in smaller nanovoids and fewer nanovoid numbers in the electroless Cu layer. Although these studies have introduced effective approaches to reducing nanovoids, the microstructure of electroless copper and the distribution of nanovoids within the microvia, prepared under various conditions, are rarely investigated.

In this work, we focused on the microstructures of the electroless Cu deposition in the Cu/electroless Cu/electrolytic Cu microvia structure under different Ni additions as well as bath temperatures. The nanovoid evolution and microstructure of the electroless Cu under different preparation conditions were characterized through TEM observations. In addition, the quantities and dimensions of the nanovoids in the electroless Cu were determined using image processing software (ImageJ) to understand the effects of Ni addition and bath temperature on nanovoid evolution. This work might shed some light on a potential approach to improve the quality of electroless Cu deposition for the microvia preparation in HDI substrate.

2. Experiment

2.1. Materials and methods

A FR4 Cu-clad laminate (Panasonic Industry Co., Ltd.) with a Cu sheet thickness of 15 ~ 20 μm was used as the base substrate in this study. To simplify the experiment, we only prepared the Cu/electroless Cu/electrolytic Cu sandwich-like structure that is identical to the microvia structure used in the HDI substrate to investigate the microstructure of electroless Cu. First, pretreatments strictly followed by conventional microvia manufacturing (Okuno Chemical Industries Co., Ltd.) were carried out to reproduce surface conditions for the electroless Cu deposition. The pretreated substrate was dipped in a prepping solution (Okuno Chemical Industries Co., Ltd.) for the Pd catalyst activation. After the FR4 Cu-clad laminate surface was well-prepared, an approximately 300 nm thick Cu layer was electroless deposited on the FR4 Cu-clad laminate surface in a chemical bath that contained Cu^{2+} 2.2 g/L from $CuSO_4{\cdot}5H_2O$ (Okuno Chemical Industries Co., Ltd.) as Cu source and formaldehyde 2 g/L (Okuno Chemical Industries Co., Ltd.) as a reducing agent under different Ni concentrations and at different bath temperatures.

Table 1 illustrates the conditions of electroless Cu plating under different Ni concentrations and reaction temperatures. Concretely, the concentration of Ni 100 % bath equals adding Ni^{2+} 150 mg/L from $NiSO_4{\cdot}6H_2O$ (Okuno Chemical Industries Co., Ltd.) in the electroless deposition bath. The Ni 100 % at 27 ℃ refers to a standard condition. The thickness of the deposition layer is about 300 nm. After electroless Cu layers were deposited separately in different conditions, a commercialized electrolytic Cu deposition was applied as microvia filing and then formed a typical Cu trace/electroless Cu/electrolytic Cu sandwich structure on the substrate. Once the sandwich structure was prepared, the substrates were annealed at 120 ℃ for 1 h to stabilize and grow the Cu grains.

2.2. Characterizations

Cross-sections of prepared substrates were polished by the ion-milling system (IM4000, Hitachi High-Tech Corporation) and observed by a focused ion beam (FIB) system (FB-2100, Hitachi High-Tech Corporation). Transmission electron microscopy (TEM), high-resolution (HR)-TEM, high-angle annular dark field scanning transmission electron microscopy (HAADF-STEM), and X-ray spectroscopy (EDS) analysis were made by using a spherical aberration corrected S/TEM (JEM-ARM200F, JEOL Ltd.) at an acceleration voltage of 200 kV. Nanovoid analysis was implemented on the image processing software (ImageJ, Fiji) [21]. The TEM images were first converted to 8-bit, then segmented using the Trainable Weka Segmentation, which applies a collection of machine learning algorithms and selected image features to produce pixel-based segmentations from Fiji's Auto Threshold plugin.

3. Results and discussion

3.1. Microstructure of electroless Cu deposition

The microstructure and elemental composition of the electroless Cu were initially investigated through TEM characterizations using the 200 % Ni incorporated electroless Cu sample. Fig. 1a depicts a HAADF-STEM image illustrating the interfacial areas among Cu trace (i), electroless Cu (ii), and electrolytic Cu (iii). Cu grains at the interfacial area exhibit a discontinuous crystalline structure. A distinct thin layer, consisting of fine Cu grains, can be differentiated between the Cu trace and the electroless Cu, which can be regarded as the electroless deposition layer. This is attributed to the added Ni being able to confine the self-diffusion of Cu because the added Ni atom tends to cumulate at the grain boundary [22]. These Ni atoms can affect the Cu grain boundaries coalescence during the annealing process, leading to the formation of a discontinuous grain growth structure with fine Cu grains.

Fig. 1b and 1c show enlarged views (250 k and 500 k) of the

Table 1
Conditions of electroless Cu deposition.

Deposition condition	Ni concertation	Bath temperature (°C)
Reduced Ni addition	50 %	27
Standard	100 %	27
Increased Ni addition	200 %	27
Increased temperature	100 %	32
Increased temperature	100 %	37

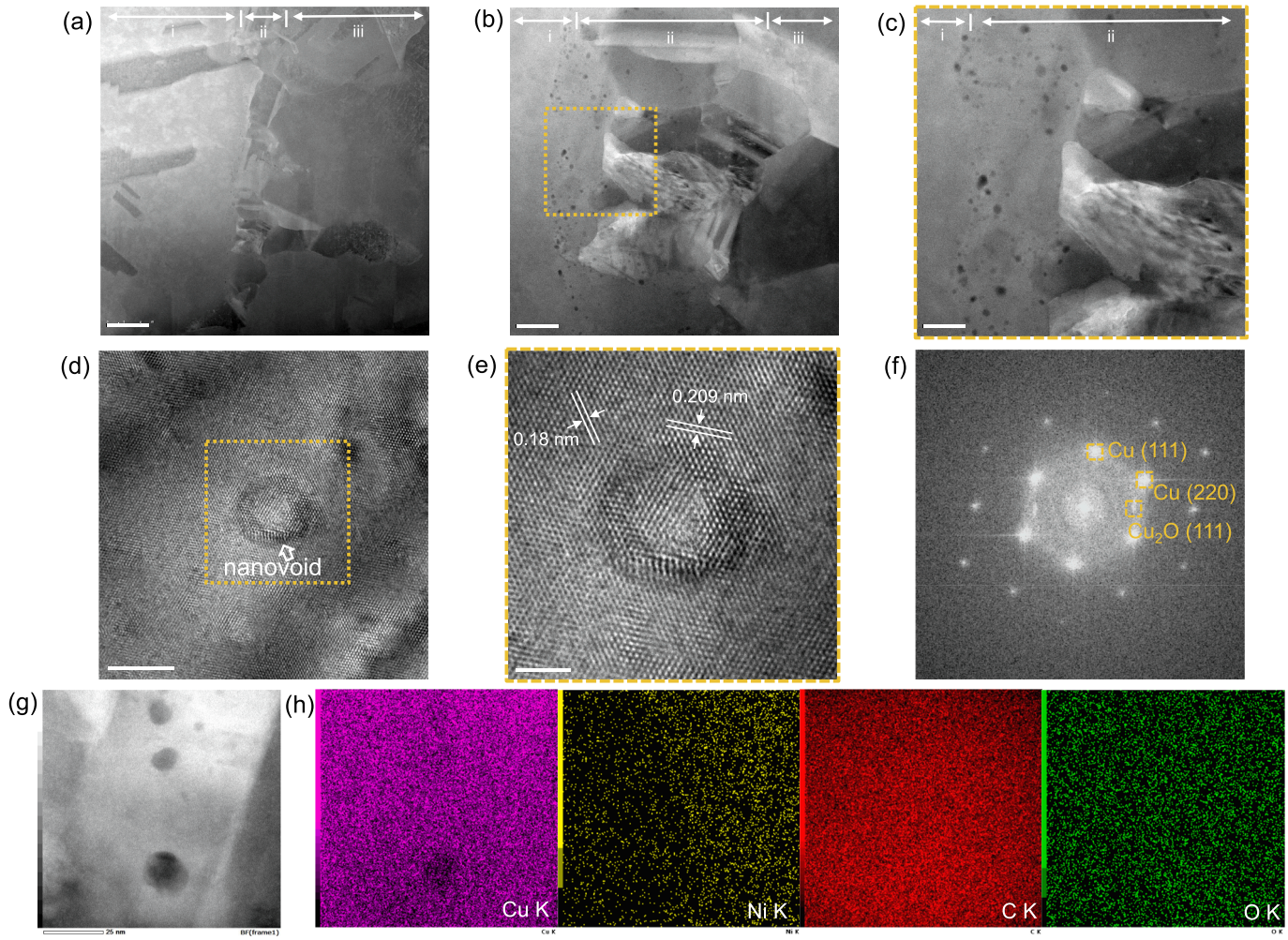

Fig. 1. HAADF-STEM images of the interfacial area among Cu trace (i), electroless Cu (ii), and electrolytic Cu (iii) at the magnifications of 50 k (a), 250 k (b), and 500 k (c). HR-TEM images of the nanovoid (d), and (e). FFT diffractogram (f) converted form (e). HAADF-STEM image of the nanovoid (g) and EDS elemental mappings (h) of Cu, Ni, C, and O.

electroless Cu layer. Massive black spots can be seen in the electroless layer, which are caused by nanovoids. These nanovoids exhibit regular round and elliptical shapes, indicating that they originated from the entrapment of H_2 bubbles during the electroless deposition rather than the vacancy formed by the fine Cu grain growth [23]. Furthermore, these nanovoids are predominantly located at the interface between the Cu trace and the electroless Cu layer. This is likely due to impurities or microscopic crevices on the surface of the Cu trace, which serve as nucleation sites where hydrogen gas can accumulate and coalesce into bubbles [24]. What is interesting to notice is that Cu grains grow epitaxially from the Cu trace to the electroless layer, and grain boundaries are mainly suited within the electroless Cu layer rather than the interface between the Cu trace and the electroless Cu. The growth of the as-deposited Cu grains was not influenced by the Ni addition because no Ni exists on the Cu trace surface. In addition, the presence of nanovoids at the interface does not impede the epitaxial growth of Cu grains, as the nanovoids are dispersively distributed in the electroless layer and the grain boundary migration can traverse the nanovoids at elevated temperatures [25].

Fig. 1d and e exhibit HR-TEM images of the nanovoid. The lattice fringes can be clearly distinguished, and there are no dislocations or grain boundaries surrounding the nanovoid, suggesting the continuous crystalline structure of Cu grain (Fig. 1d). Lattice fringes with spacings of 0.18 nm and 0.209 nm were identified in Fig. 1e, which correspond to the Cu (220) and (111) planes, respectively. Fig. 1f is the fast Fourier transform (FFT) of the HR-TEM image of 1e. The diffraction patterns are well-matched with a typical diffraction pattern of Cu. In addition, the lattice fringe is also determined as the Cu_2O (111) plane in Fig. 1e, which is attributed to the oxidation of the surface of Cu matrix arising from TEM sampling process.

The elemental compositions around the nanovoid were further confirmed through EDS mapping. Fig. 1g is a HAADF-STEM image of the nanovoids located at the interface between the Cu trace and the electroless Cu layer, on which the EDX mapping was introduced. The intensity of Cu K-line is weak around the black spots, indicating the presence of the hollow structure in the black spot area (Fig. 1h). The Ni-K line displays a higher intensity at the right side of the nanovoid due to the addition of Ni in the electroless layer. Although C and O were detected and found to be uniformly distributed throughout the entire image, there is no obvious agglomeration of these elements near these nanovoids. From the above EDS results, the inside of nanovoids can be derived as a hollow structure.

3.2. *Reaction rate under different conditions*

The deposition rate of electroless Cu under different concentrations of Ni addition and temperature conditions were calculated and listed in Table 2. Effect of Ni addition on the electroless Cu deposition rate was investigated by the samples with 50 %, 100 %, and 200 % Ni addition at the reaction temperature of 27 °C. The temperature effect on the

Table 2
Electroless Cu deposition rate under different conditions.

Deposition conditions		Bath temperature		
		27 °C	32 °C	37 °C
Ni concentration	50 %	11.87 nm/min		
	100 %	13.60 nm/min	23.75 nm/min	32.53 nm/min
	200 %	1 nm/min		

electroless Cu deposition was also considered at 27 °C, 32 °C, and 37 °C, respectively. According to the results, both increasing Ni addition concentration and bath temperature can boost the Cu deposition rate, whereas the increase in the bath temperature reveals remarkable effects on the deposition rate. The deposition rate only increased by about 32 % when the Ni concentration increased from 50 % to 200 %, whereas the deposition rate increased by 139 % after the bath temperature increased to 37 °C. It has been reported that the addition of Ni during electroless Cu deposition can boost the reaction rate due to a synergetic effect [15]. However, the chemical reactions are much more sensitive to the reaction temperature and can be exponentially increased with an elevated temperature. The microstructures of the Cu deposition layer were then investigated separately based on the Ni addition and temperature effects.

3.3. Ni addition effect on Cu electroless layer

The Ni effect on the Cu microstructure of the microvia was investigated by using the scanning ion microscope (SIM) images as shown in Fig. 2. Compared to the conventional scanning electron microscopy (SEM), SIM images own pronounced crystallographic contrast information due to ion-channeling effect, which is beneficial for distinguishing grain boundaries and interfaces. It can be seen that all the cross-sectional structures (Fig. 2a, c, and e.) own large Cu grains with various orientations after preparation. In the sample with 50 % Ni (Fig. 2a), Cu grains show an epitaxially crystallized structure from the Cu trace to the electrolytic Cu. There is no distinguishable interface between the Cu trace and the electrolytic Cu layer. A magnified image of the interfacial area is shown in Fig. 2b. The thin electroless Cu layer cannot be further identified, illustrating that the electroless Cu has been completely merged into the structure due to grain growth during the annealing. However, as the Ni addition increases to 100 %, slight changes can be identified in the interfacial areas between the Cu trace and the electrolytic Cu as shown in Fig. 2c and d. Although continuous grain growth is still evident in most interfacial areas, an interface can be seen between the electrolytic Cu and the Cu trace in specific regions. The formation of the interface can be attributed to the increased Ni addition that not only can prevent the interdiffusion among fine Cu grains but also impedes the epitaxial grain growth from the electroless Cu to the electrolytic Cu. The effect of Ni becomes more pronounced in the sample with a 200 % Ni addition. In this case, an obvious interface caused by the discontinuous growth of Cu grains (Fig. 2e). In addition, there is an area featuring a fine Cu grain cluster and tiny voids as shown in Fig. 2f. Interdiffusion and recrystallization of the Cu grains are further prohibited due to the higher Ni addition, which results in such a fine Cu grain cluster in the electroless Cu layer even after annealing at 120 °C.

HAADF-STEM observations were also carried out to investigate the microstructure of the electroless Cu layer. Fig. 3a-3c show the cross-sectional HAADF-STEM images of the sample prepared at 50 %, 100 %, and 200 % Ni addition at a magnification of 250 k, respectively. Black spots are identified in the HAADF-STEM images, illustrating the existence of nanovoids in the electroless layer. The samples with 50 % and 100 % Ni addition show an epitaxial growth structure from the Cu trace to the electrolytic Cu, whereas the sample with 200 % Ni concentration exhibits discontinuous grain growth with fine Cu grains in the electroless layer. Fig. 3e-3g exhibit the enlarged HAADF-STEM images (500 k) of samples prepared under 50 %, 100 %, and 200 % Ni addition. Circular and elliptical nanovoids are present in the electroless layer, and most of the larger nanovoids are primarily situated at the interface between the Cu trace and the electroless layer, forming a nanovoid line. This can be ascribed to inadequate cleaning and rough surface structure of the Cu

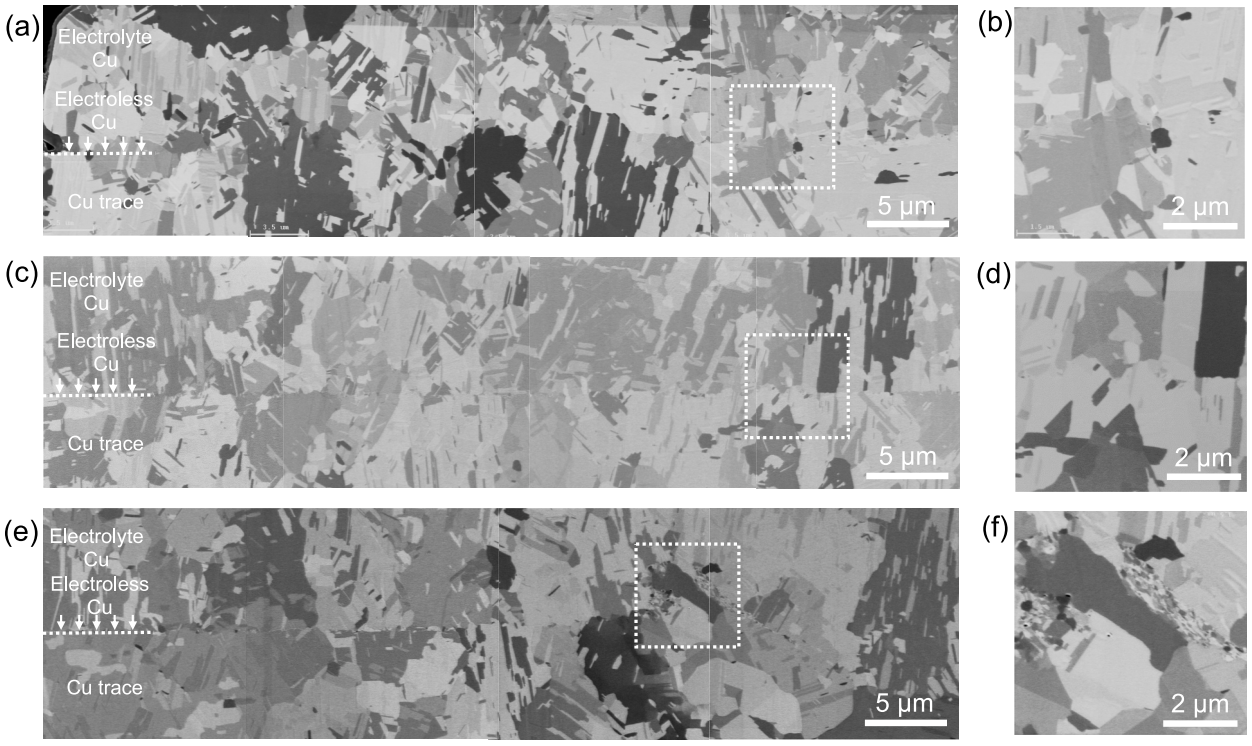

Fig. 2. SIM images of the Cu trace/electroless Cu/electrolytic Cu structure with 50% (a), 100% (c), and 200%(e) Ni addition in the electroless Cu. Enlarged views of the interfacial areas of 50%(b), 100% (d), and 200%(f) Ni addition in the electroless Cu.

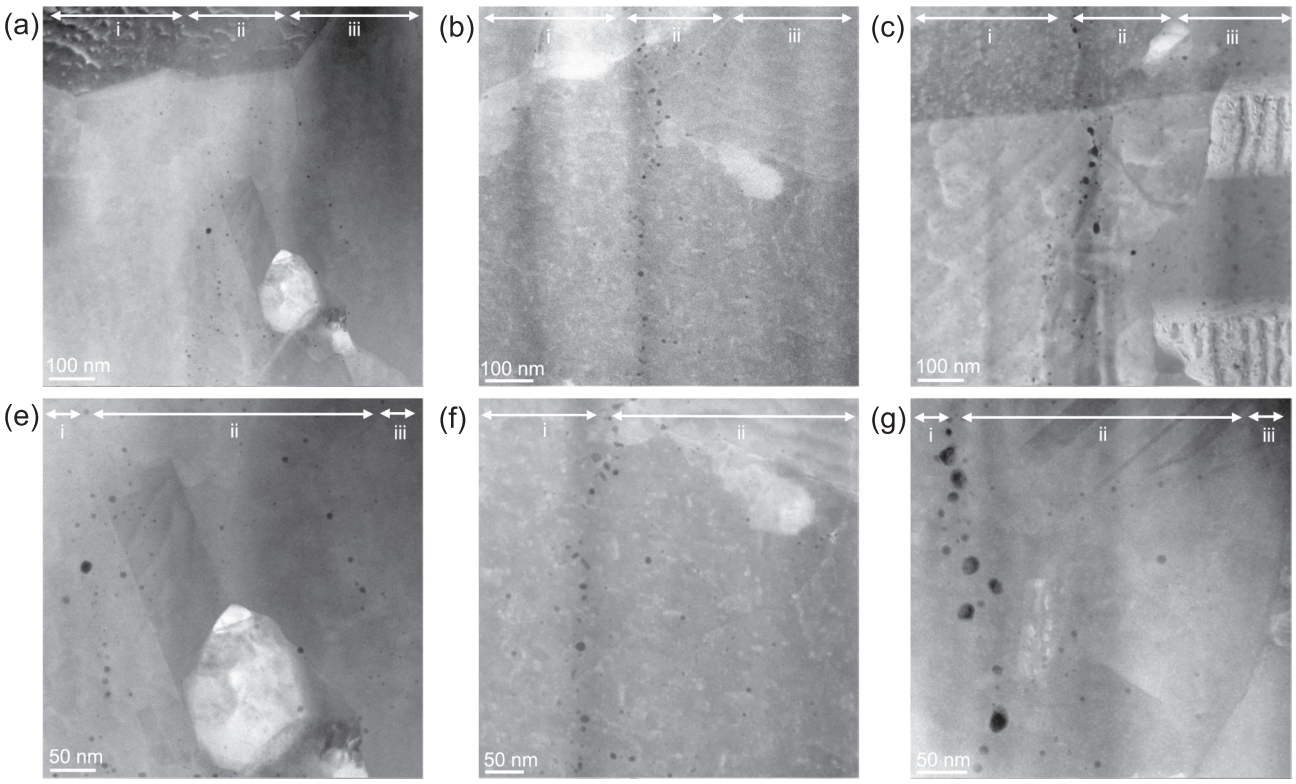

Fig. 3. Cross-sectional HAADF-STEM images of the interfacial areas (i: Cu trance; ii: electroless Cu; iii: electrolytic Cu) of prepared samples with 50 % (a) (e), 100 % (b) (f), and 200 % (c) (g) with a magnification of 250 k and 500 k, respectively.

trace where the hydrogen bubbles nucleate at the remaining impurities and crevices. This formed nanovoid line can be regarded as a potential failure risk for the HDI substrate, resulting in cracking and delamination in the microvias. Furthermore, the size of the nanovoid increases with the Ni concentration, which will be further elaborated in section 3.5.

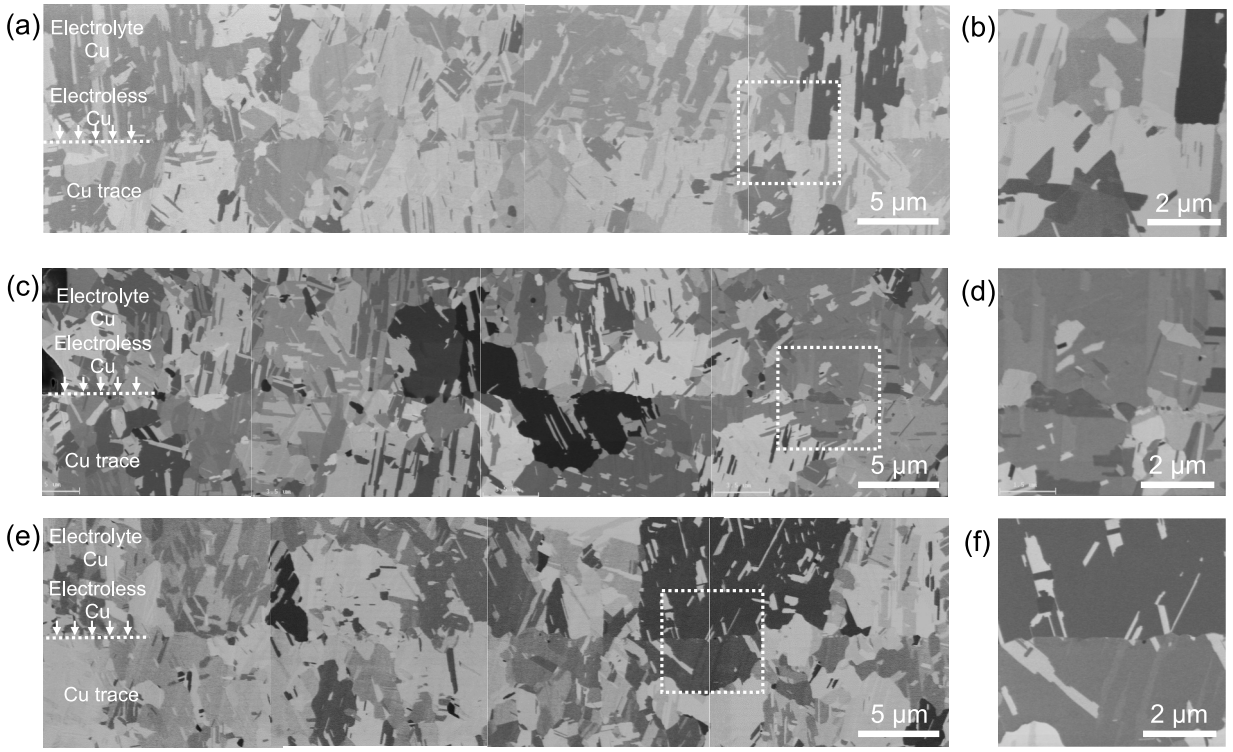

Fig. 4. Cross-sectional SIM images of the Cu trace/electroless Cu/electrolytic Cu structure with the electroless Cu prepared at 27°C (a), 32°C (c), and 37°C (e), and enlarged views of the interfacial areas (b), (d), and (f), respectively.

3.4. Temperature effect on Cu electroless layer

The influence of bath temperature on the microstructure was investigated through the samples prepared at 27 °C, 32 °C, and 37 °C with the 100 % Ni addition. Cross-sectional SIM images of the samples are shown in Fig. 4. It can be observed that all specimens exhibit a similar crystalline structure, consisting of large Cu grains with varying orientations. Additionally, both the epitaxial and non-epitaxial Cu grains can be distinguished at the Cu trace/electroless Cu/electrolytic Cu interfaces. Fig. 4b, 4d, and 4f depict the magnified images of the corresponding samples. The thin electroless has completely disappeared after annealing and there are no such fine Cu grains observed at the interfacial area. The similar crystalline structure of all samples suggests that the electroless Cu bath temperatures have little effect on the Cu grain growth and interfacial structure.

Fig. 5 shows the HAAD-STEM observations of electroless Cu layers prepared at 32 °C and 37 °C. The elliptical and circular black dots can be clearly distinguished in the electroless copper layer, illustrating the presence of nanovoids. Similar to the observation in Fig. 3. These nanovoids are sequentially arranged at the interface between the Cu trace and electroless layer. The crystalline structure reveals continuous grain growth from the Cu trace to the electrolytic Cu, indicating the interface is not changed due to the presence of nanovoids. Magnified observations of the interface are shown in Fig. 6c and 6d. Large nanovoids mainly appear at the interface whereas the smaller nanovoids are more prevalent in the Cu electroless layer. It is also worthwhile noticing that the size of the nanovoids increases as the bath temperature increases. The details will be discussed in section 3.5.

3.5. Relationship between size and reaction rate

To comprehend the impacts of different reaction conditions on the formation of nanovoids, we measured the maximum caliper diameter of nanovoids by using ImageJ and analyzed the nanovoid size distribution under different preparation conditions. Fig. 6a-6c exhibit the HAADF-STEM images of the samples in 50 %, 100 %, and 200 % Ni addition, alongside their corresponding black-and-white converted images, respectively. All HAADF-STEM images were successfully converted into black-and-white images, where the white area corresponds to the background and the black dots indicate the nanovoids. It can be observed that the size of the nanovoids increases with higher Ni incorporation, while the number of nanovoids decreases, as indicated by the reduced number of black dots.

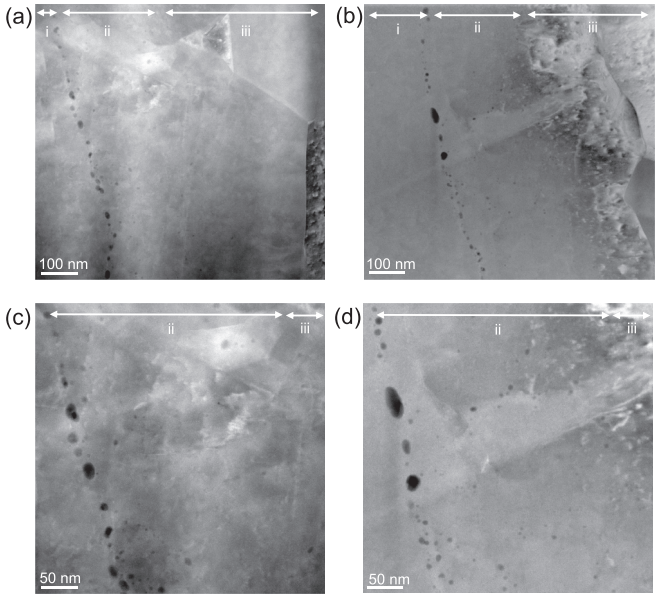

Fig. 5. Cross-sectional HAADF-STEM images of the interfacial area (i: Cu trace; ii: electroless Cu; iii: electrolytic Cu) of prepared samples at 32 °C (a) (c), and 37 °C (b) (d) with a magnification of 250 k and 500 k, respectively.

Fig. 6d-6f illustrate the histogram representing the nanovoid size distribution in samples with varying concentrations of Ni determined from the black-and-white processed images. In the case of 50 % Ni incorporated sample, 433 nanovoids have been counted, with the average size of them being about 3.7 nm. Over 40 % of nanovoids are 2 ~ 3 nm and the majority of nanovoids have a size of less than 10 nm. For the sample with 100 % Ni addition, 199 nanovoids have been differentiated in the converted black-and-white image and the average size of these nanovoids is about 5.8 nm. Although nanovoids with a size from 2 ~ 3 nm exhibit the highest occurrence frequency according to the histogram, large nanovoids with a size over 10 nm have extensively emerged. As the Ni addition increases to 200 %, the highest occurrence frequency shifts to 4 ~ 5 nm, and the average size of the nanovoids increases to 6.7 nm, while the number of them has been significantly reduced to 167.

Meanwhile, the samples prepared under different bath temperatures were also investigated to assess the temperature impacts on the formation of nanovoids. As shown in Fig. 7a and 7b massive black dots that signify the nanovoids have been identified, which are located in the Cu electroless layer. Large nanovoids concentrate at the interface between the Cu trace and the electroless layer, forming a visible line along with the interface. However, small nanovoids are prevalent throughout the electroless layer, distributed randomly. The size distribution of the nanovoids in the samples prepared at different temperatures is shown in Fig. 8c and d. As the reaction temperature increases to 32 °C, 184 nanovoids are observed in the field of view, and the size of the nanovoids increases and the peak of the histogram appears at the range of 4 ~ 5 nm. In the case of the sample prepared at 37 °C, although there are appreciable large nanovoids observed in the HAADF-STEM images, the highest peak still appears at the range of 2 ~ 3 nm. This may be attributed to the fact that larger bubbles are easier to release during the deposition process compared to smaller bubbles, as they experience a greater buoyant force due to their larger volume.

The relationships between Cu deposition rate and nanovoid porosity, average diameter, and maximal diameter were investigated and plotted in Fig. 8a-8c, respectively. The electroless Cu with the slowest deposition rate has the lowest porosity, measuring at just 1 %. The sample prepared with the highest deposition rate exhibits a porosity of 2 %, exhibiting 100 % increase in porosity compared to the lowest deposition rate sample. The relationship between deposition rate and average diameter follows an asymmetric parabolic curve. The average size of the nanovoids increases significantly with a higher deposition rate, reaching a peak under reaction conditions at 32 °C with a Ni concentration of 100 %. However, the nanovoid size exhibits a slight decrease as the deposition rate continues to increase. The maximal diameter of the nanovoid increases with the increase in deposition rate and remains stable with a diameter of about 50 nm. The relationships indicate that the size of the nanovoids is strongly related to the reaction rate of the electroless Cu deposition. In the case of low reaction temperature or low concentration of Ni, the reaction is comparatively slow, thereby suppressing the generation of hydrogen gas. Consequently, only a few small hydrogen bubbles are entrapped in the electroless layer, forming tiny nanovoids in the deposition layer under these slower reaction conditions. As the reaction accelerates, larger hydrogen bubbles are generated and attach to the surface, leading to the formation of larger nanovoids. However, as the size of the hydrogen bubbles increases, the higher buoyant force acting on the larger bubbles allows them to detach more easily from the deposition surface compared to smaller bubbles.

4. Conclusions

In this work, we investigated the effects of Ni addition and deposition

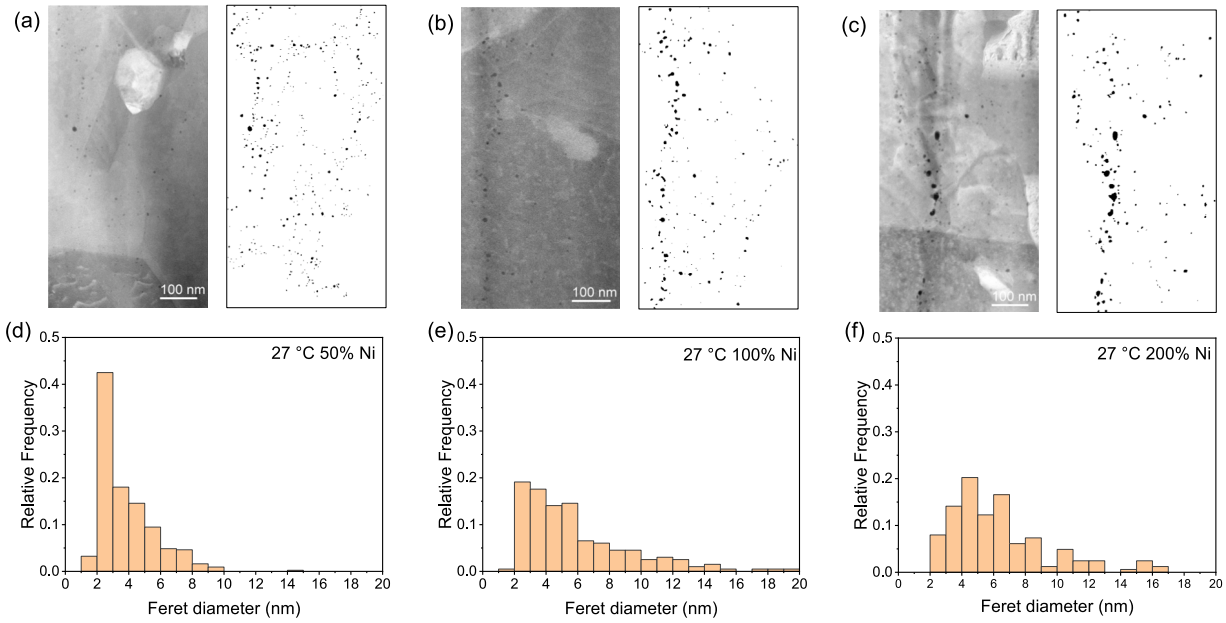

Fig. 6. Cross sectional HAADF-STEM images and corresponding black-and-white processed image of the sample with 50% (a), 100% (b), and 200% (c) Ni addition. Histogram of the diameter of the nanovoids calculated from the black-and-white processed images (d)-(f).

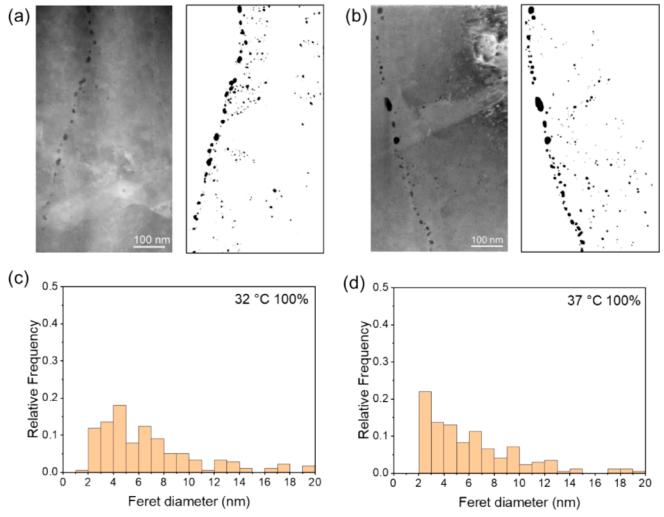

Fig. 7. Cross-sectional HAADF-STEM images and corresponding black-and-white processed images of the sample prepared at 32 °C (a) and 37 °C (b). Histogram of the diameter of the nanovoids calculated from the black-and-white processed images (c) and (d).

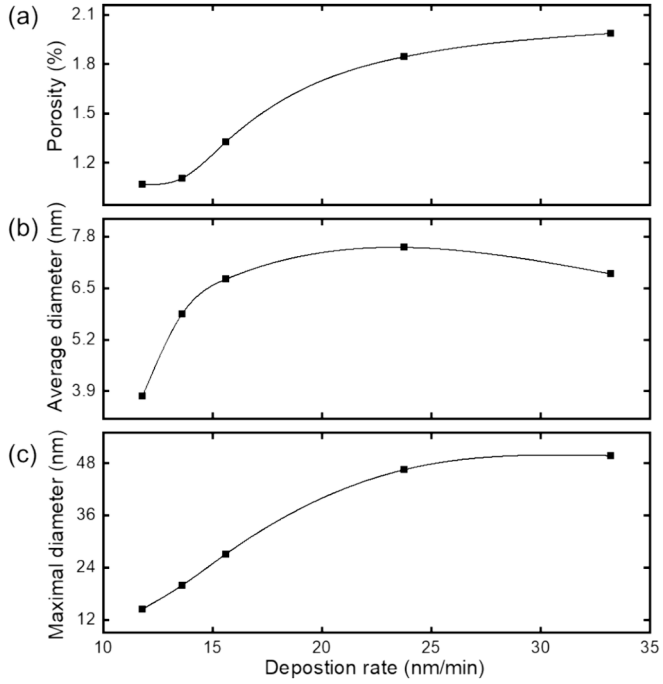

Fig. 8. Relationship between Cu deposition rate and porosity (a), average diameter (b), and maximal diameter (c).

temperature on the microstructure of electroless Cu. The addition of Ni during deposition significantly affects the crystalline structure of the electroless layer in the Cu trace/electroless Cu/electrolyte Cu structure. Epitaxial grain growth from the Cu trace to the electrolytic Cu is severely impeded by the electroless Cu layer when the Ni addition reaches 200 %, while variations in deposition temperature show no noticeable influence on the crystalline structure of Cu. The evolution of nanovoids under different deposition conditions was also investigated and analyzed using TEM and ImageJ software. Nanovoids extensively exist in the electroless layer, which is caused by the encapsulation of H_2 bubbles during electroless deposition. However, these nanovoids have a negligible effect on the epitaxial grain growth of Cu, as the grain boundary migration can traverse the nanovoids during the annealing process. As the deposition rate increases, the size and porosity of the nanovoids in the electroless layer increase significantly, stabilizing once the deposition rate exceeds 23.75 nm/min. This is attributed to the increase in H_2 bubble size with the deposition rate. As the size of the H_2 bubbles increases further at higher rates, larger bubbles tend to detach from the deposition surface, halting any further increase in nanovoid size. This work provides insights into potential approaches for improving the quality of electroless Cu deposition for microvia preparation in HDI substrates.

CRediT authorship contribution statement

Zheng Zhang: Writing – review & editing, Writing – original draft, Investigation, Formal analysis, Data curation, Conceptualization. **Ming-**

Chun Hsieh: Writing – review & editing, Software, Investigation. **Masahiko Nishijima:** Writing – review & editing, Visualization, Software, Methodology. **Aiji Suetake:** Resources. **Hiroshi Yoshida:** Project administration. **Rieko Okumuara:** Software, Methodology. **Chuantong Chen:** Project administration. **Hiroki Seto:** Resources, Methodology, Investigation. **Kei Hashizume:** Project administration. **Yuhei Kitahara:** Methodology, Investigation. **Haruki Nagamura:** Methodology, Investigation. **Katsuaki Suganuma:** Project administration, Funding acquisition.

Declaration of competing interest

The authors declare that they have no known competing financial interests or personal relationships that could have appeared to influence the work reported in this paper.

Data availability

Data will be made available on request.

Acknowledgements

This paper is based on results obtained from the project from "Research and Development Project of the Enhanced Infrastructures for Post-5G Information and Communication Systems" JPNP20017, subsidized by the New Energy and Industrial Technology Development Organization (NEDO) and partly supported by "Crossover Alliance to Create the Future with People, Intelligence and Materials" from MEXT, Japan. The author also acknowledges the Comprehensive Analysis Center of Osaka University for the use of TEM.

References

[1] Y. Ma, L. Guo, L. Qi, J. Sun, J. Wang, Y. Cao, Growth mechanism and thermal behavior of electroless Cu plating on short carbon fibers, Surf Coat Technol 419 (2021) 127294, https://doi.org/10.1016/j.surfcoat.2021.127294.
[2] F. Inoue, H. Philipsen, A. Radisic, S. Armini, Y. Civale, P. Leunissen, M. Kondo, E. Webb, S. Shingubara, Electroless Cu deposition on atomic layer deposited Ru as novel seed formation process in through-Si vias, Electrochim Acta 100 (2013) 203–211, https://doi.org/10.1016/j.electacta.2013.03.106.
[3] X.-Q. Cheng, P.-F. Shi, Electroless Cu-plated Ni_3Sn_4 alloy used as anode material for lithium ion battery, J Alloys Compd 391 (2005) 241–244, https://doi.org/10.1016/j.jallcom.2004.08.080.
[4] M. Cauwe, B. Vandevelde, C. Nawghane, M. Van De Slyeke, A. Coulon, S. Heltzel, Challenges in introducing high-density interconnect technology in printed circuit boards for space applications, CEAS Space Journal 15 (2023) 101–112, https://doi.org/10.1007/s12567-021-00403-2.
[5] K. Zeng, J. Williamson, Improve Interconnect Reliability of BGA Substrate with Stacked Vias by Reducing Carbon Inclusion in the Interface Between Via and Land Pad, in: 2018 IEEE 68th Electronic Components and Technology Conference (ECTC), IEEE, 2018: pp. 150–156. doi: 10.1109/ECTC.2018.00031.
[6] M. Cauwe, B. Vandevelde, C. Nawghane, M. Van De Slyeke, E. Bosman, J. Verhegge, A. Coulon, S. Heltzel, High-Density Interconnect Technology Assessment of Printed Circuit Boards for Space Applications, J. Microelectron. Electron. Packag. 17 (2020) 79–88, https://doi.org/10.4071/imaps.1212898.
[7] Interface (2018).
[8] Ivan Straznicky, Bill Birch, Joe Smetana, Reliability testing of multiple level microvia structures following exposure to lead-free assembly, in: SMTA International 2017, 2017.
[9] S. Nakahara, Y. Okinaka, Microstructure and ductility of electroless copper deposits, Acta Metall. 31 (1983) 713–724, https://doi.org/10.1016/0001-6160(83)90086-X.
[10] T. Sharma, A.E. Landry, A. Leger, D.A. Brown, T. Bernhard, S. Zarwell, F. Brüning, R. Brüning, Nickel dependence of hydrogen generation, hydrogen co-deposition and film stress in an electroless copper process, Thin Solid Films 666 (2018) 76–84, https://doi.org/10.1016/j.tsf.2018.09.029.
[11] T. Bernhard, F. Brüning, R. Brüning, T. Sharma, D. Brown, S. Zarwell, C. Bishop, The Impact of Hydrogen Gas Evolution on Blister Formation in Electroless Cu Films, J. Microelectron. Electron. Packag. 12 (2015) 86–91, https://doi.org/10.4071/imaps.458.
[12] S. Nakahara, Microscopic mechanism of the hydrogen effect on the ductility of electroless copper, Acta Metall. 36 (1988) 1669–1681, https://doi.org/10.1016/0001-6160(88)90234-9.
[13] S. Nakahara, Y. Okinaka, Microstructure and Mechanical Properties of Electroless Copper Deposits, Annu. Rev. Mater. Sci. 21 (1991) 93–129, https://doi.org/10.1146/annurev.ms.21.080191.000521.
[14] J.E.A.M. Van Den Meerakker, On the mechanism of electroless plating. II. One mechanism for different reductants, J Appl Electrochem 11 (1981) 395–400, https://doi.org/10.1007/BF00613960.
[15] J.E.A.M. van den Meerakker, J.W.G. de Bakker, On the mechanism of electroless plating. Part 3. Electroless copper alloys, J Appl Electrochem 20 (1990) 85–90, https://doi.org/10.1007/BF01012475.
[16] J.-W. Seo, H.-S. Nam, S. Lee, Y.S. Won, Prevention of blister formation in electrolessly deposited copper film on organic substrates, Korean J. Chem. Eng. 29 (2012) 529–533, https://doi.org/10.1007/s11814-011-0208-0.
[17] T. Bernhard, E. Steinhauser, S. Kempa, G. Krilles, R. Massey, F. Bruning, Nickel dependence of hydrogen co-deposition and nanoporosity in electrolessly deposited Cu-films, in: 2020 IEEE 70th Electronic Components and Technology Conference (ECTC), IEEE 2020 (2020) 735–741, https://doi.org/10.1109/ECTC32862.2020.00121.
[18] J.E.A.M. Van Den Meerakker, On the mechanism of electroless plating. I. Oxidation of formaldehyde at different electrode surfaces, J Appl Electrochem 11 (1981) 387–393, https://doi.org/10.1007/BF00613959.
[19] Z. Zhang, M.-C. Hsieh, R. Liu, J. Yeom, A. Suetake, H. Yoshida, C. Chen, J. Kang, H. Honma, Y. Kitahara, T. Matsunami, K. Otsuka, K. Suganuma, Effect of electroless Cu depositions for micro-via structure and thermal cycling reliability, Microelectron. Reliab. 138 (2022) 114707, https://doi.org/10.1016/j.microrel.2022.114707.
[20] S.-Y. Park, H.-W. Cha, J.-W. Joung, C.-W. Yang, Quantification of the Nano-Voids in Electroless Deposited Copper Layers Using SiNx TEM Grids, J Electrochem Soc 168 (2021) 102504, https://doi.org/10.1149/1945-7111/ac2bec.
[21] https://imagej.net/software/fiji/, Fiji 2.15.1, Windows 64-Bit (2024).
[22] E. Logan, T. Sharma, F. Brüning, S. Zarwell, E. Steinhäuser, T. Bernhard, N. Chen, R. Brüning, The effect of Ni on the kinetics of electroless Cu film deposition, Thin Solid Films 626 (2017) 131–139, https://doi.org/10.1016/j.tsf.2017.02.026.
[23] C. Fan, H. Wang, X. Zhang, Nanovoid formation mechanism in nanotwinned Cu, Discover Nano 19 (2024) 43, https://doi.org/10.1186/s11671-024-03984-z.
[24] S.F. Jones, G.M. Evans, K.P. Galvin, Bubble nucleation from gas cavities — a review, Adv Colloid Interface Sci 80 (1999) 27–50, https://doi.org/10.1016/S0001-8686(98)00074-8.
[25] L. Zhang, Y. Shibuta, C. Lu, X. Huang, Interaction between nano-voids and migrating grain boundary by molecular dynamics simulation, Acta Mater. 173 (2019) 206–224.